An experimental and theoretical investigation of the electronic structure of CdO

1998 J. Phys.: Condens. Matter 10 8447

(http://iopscience.iop.org/0953-8984/10/38/006)

J. Phys.: Condens. Matter **10** (1998) 8447–8458. Printed in the UK PII: S0953-8984(98)93531-7

An experimental and theoretical investigation of the electronic structure of CdO

Y Dou†, R G Egdell†‖, D S L Law‡, N M Harrison§ and B G Searle§

† Inorganic Chemistry Laboratory, South Parks Road, Oxford OX1 3QR, UK
‡ Research Unit for Surfaces Transforms and Interfaces, Daresbury Laboratory, Warrington, Cheshire WA4 4AD, UK
§ CLRC Daresbury Laboratory, Warrington, Cheshire, WA4 4AD, UK

Received 22 April 1998, in final form 15 July 1998

Abstract. Photoemission spectra of polycrystalline CdO have been measured under excitation with monochromatic x-rays and with variable energy UV radiation from a synchrotron source. Experimental data are compared with density of states profiles calculated by periodic Hartree–Fock and density functional methods. Both calculations suggest that there is significant mixing between Cd 4d and O 2p states, but the Hartree–Fock calculations better reproduce the experimental O 2p to Cd 4d separation and the O 2p bandshape. Constant initial state profiles measured with variable photon energy in the range between 30 eV and 100 eV provide experimental evidence for O 2p–Cd 4d mixing.

1. Introduction

CdO is unique amongst IIB-VI compounds in that it adopts a face-centred-cubic rocksalt structure based on octahedral coordination around Cd. The wurtzite and zinc blende structures of the other Cd and Zn chalcogenides, including ZnO, are all based on tetrahedrally coordinate metal cations. In contrast to these materials, the lowest energy bandgap of CdO is indirect with a quoted transition energy of 0.55 eV at room temperature and 0.84 eV at 100 K [1]. This energy is much lower than the lowest gaps for CdS (2.485 eV), CdSe (1.751 eV) and CdTe (1.475 eV) [1]. In isostructural series of compounds with a common cation, the bandgap usually decreases monotonically in moving from the oxide to the telluride. The bandgaps in the series CdO (0.55 eV), In_2O_3 (3.750 eV) [2], SnO_2 (3.60 eV) [3] also show an irregular variation that contrasts with the monotonic decrease found in more typical series such as CaO (6.93 eV) [4], Sc_2O_3 (6.00 eV) [5], TiO_2 (3.06 eV) [6]. The bandgap of CdO must therefore be regarded as anomalously low.

Interest in the electronic structure of CdO has prompted at least five bandstructure calculations [7–11], the most recent of which is due to Kunz and coworkers [11]. These authors used a Hartree–Fock approach corrected to allow for electron correlation to compute the energy bands for rocksalt CdO, as well as for ZnO in its ambient wurtzite and high-pressure rocksalt modifications. Indirect bandgaps in the rocksalt phases were shown to arise from interaction between shallow core d states (3d for ZnO and 4d for CdO) and valence band O 2p states. There is inversion symmetry at the zone centre (Γ) in the rocksalt structure where the point group is O_h. This means that there can be no mixing

‖ Corresponding author. E-mail address: russ.egdell@chemistry.ox.ac.uk.

0953-8984/98/388447+12$19.50

between O 2p and Cd 4d states at this point because they have different parity. Equally there is no mixing with Cd 5s conduction band states. However, away from Γ mixing is allowed. The interaction between the inner Cd 4d states and the O 2p valence band states pushes some O 2p states upward as one moves away from the zone centre. This effect was found to produce at least three maxima in the O 2p bands, located at the L point, close to the zone centre along ΓX and midway along ΓK.

The energy separation between O 2p and Cd 4d levels is crucial in determining the magnitude of the interaction between these states. There is, however, a paucity of experimental data for electronic energy levels in CdO. The earlier band calculations invariably make reference to a paper published in 1971 [12] to define the experimental location of the Cd 4d states. However, the data reported in this earlier work were gathered under very poor vacuum conditions and the energy referencing of the spectra is not well defined. In the present communication we present high-resolution valence band x-ray photoemission spectra (XPS) of CdO excited with monochromated Al K_α radiation. The spectral data are compared with cross section weighted partial density of state profiles derived from Hartree–Fock calculations and from density functional theory. Both calculations confirm that there is pronounced O 2p–Cd 4d mixing. The simplicity of the structure of CdO makes it an ideal material in which to explore the scope and limitations of current theoretical approaches to solid-state electronic structure.

The issue of mixing between shallow core nd levels and outer 'ligand' based n'p valence levels in compounds of Zn, Cd and Hg has been of broader interest in the chemical literature for many years. For example, the propensity of Hg to adopt linear coordination in molecular and solid-state environments is often attributed to 'involvement' of the 5d levels in bonding [13]. However, the more tightly bound 3d and 4d levels of Zn and Cd were assumed to be 'disengaged' from covalent mixing with outer valence levels in the earlier chemical literature [14] and in early bandstructure calculations on ZnO [15, 16]. One experimental approach to probing the hybridization of inner d levels with outer valence is to explore variations in photoionization cross sections with photon energy for the inner nd shells and the outer n'p valence levels [17]. The cross section profiles for atomic nd shells show a pronounced maximum well above threshold due to centrifugal barrier effects [18]. By contrast profiles for pure atomic n'p valence shells generally fall off rapidly just above threshold [18]. Thus mixing between nd and n'p states will manifest itself in terms of a maximum in the outer valence level cross section profile that provides an echo (possibly weak) of the maximum for the inner nd shell. We exploit this idea in the present paper by using synchrotron radiation to measure ionization cross section profiles for the O 2p valence band and Cd 4d states in CdO. These experiments provide additional confirmation of significant involvement of the Cd 4d levels in the valence band states of CdO.

2. Computation

All calculations were performed using the package CRYSTAL95 [19]. The single-particle orbitals of the periodic system were expanded in a linear combination of atomic orbitals (LCAO). The exchange and correlation potentials were treated using both the exact exchange interaction (Hartree–Fock theory) and density functional theory (DFT) implemented within the local density approximation (LDA) [20, 21].

The radial variations of atomic orbitals are expressed in terms of a basis set consisting of linear combinations of Gaussian-type functions. The basis sets used were of triple valence quality: each occupied orbital in the valence region was described by three independent functions. The cadmium ion was represented by a basis set 9-7-6-311-D631G20 [22], with

the outer exponents variationally optimized with respect to the energy of an isolated Cd^{2+} ion. The oxygen basis set, 8-411G*, was that used previously in studies of magnesium oxide [23].

The convergence of the real-space summations of the Coulomb and exchange contributions to the Hamiltonian are controlled by five overlap criteria (T1–T5). The control of these approximations is described in detail elsewhere [19]. In order to converge the eigenvalues to an accuracy better than 1 mHa, these tolerances were set to 10^{-8}, 10^{-8}, 10^{-8}, 10^{-8} and 10^{-16} in the current study.

All calculations were performed using the experimental lattice parameter of 4.700 Å measured for the sample used in the present study. Interpretation of the electronic structure has been aided by a Mulliken partitioning scheme which has been used to provide atom-projected densities of states [19].

3. Experiment

High-purity polycrystalline CdO (99.999%, Fluorochem) was annealed in air at 880 °C for 2 days, pressed into pellets between tungsten carbide dies and then further sintered at 800 °C for 8 h to yield robust ceramic pellets. XPS were measured in a Scienta ESCA 300 spectrometer. This incorporates a rotating anode x-ray source, a 7 crystal x-ray monochromator and a 300 mm mean radius spherical sector electron energy analyser with parallel electron detection system. The x-ray source was run with 200 mA emission current and 14 kV anode bias, whilst the analyser operated at 150 eV pass energy with 0.5 mm slits. Gaussian convolution of the analyser resolution with an effective linewidth of 260 meV for the x-ray source gives an effective instrument resolution of 350 meV. Binding energies are referenced to the Fermi energy of an ion bombarded silver foil which is regularly used to calibrate the spectrometer. Samples were cleaned by heating pellets in the preparation chamber of the spectrometer (base pressure 10^{-9} mbar) using a VG P8 probe operating at 500 °C (probe temperature) for 5 h. The pellets were subsequently bombarded with 600 eV argon ions at a flux of around 10 μA cm^{-2} for 15 min, followed by re-annealing at 500 °C. The cleaning procedure reduced the C 1s/O 1s intensity ratio to below 0.01. There was no indication of subsequent contaminant build-up during the XPS measurements.

UV photoemission measurements were carried out on beamline 6.2 of the synchrotron radiation source of the Daresbury Laboratory. The beamline incorporates a monochromator with two sets of toroidal gratings covering the photon energy ranges 15–40 eV (710 lines/mm) and 40–140 eV (1800 lines/mm). The electron energy analyser has 150° spherical sector deflection elements of mean radius 50 mm. Energy distribution curves (EDCs) were recorded at 10 eV pass energy with 1 mm slits and 3.3° entrance half-angle. The photon bandwidth was fixed at 0.1 eV. Under these conditions the overall experimental resolution is about 0.15 eV. Constant initial state (CIS) spectra were recorded by varying the photon energy and electron kinetic energy in synchrony to maintain a constant initial state. The photon bandwidth was degraded to 0.2 eV and the pass energy was increased to 20 eV in these experiments. Count rates were normalized relative to the drain current from a tungsten mesh beam monitor through which the synchrotron beam passed just prior to hitting the sample. The CIS curves were further corrected for the quantum efficiency of the beam monitor mesh. All spectra were recorded in normal emission with radiation incident at 45° to the sample surface. The cleaning procedure was similar to that used in the Scienta spectrometer.

4. Results and discussion

4.1. Theoretical band structures and partial densities of states

The band structure derived from the Hartree–Fock calculation is shown in figure 1 along the high-symmetry directions ΓX, XK, KΓ and ΓL. The topology of the bands is similar to earlier calculations [11]. Key features of the band structure are summarized in table 1. It is found that there is pronounced mixing between the Cd 4d and O 2p states along the ΓL direction so that the topmost oxygen band shows strong upward dispersion and the L_3 band at the L point lies 1.25 eV above Γ_{15} at Γ. A second maximum is found roughly midway along ΓK in the Σ_4 band, with the maximum 1.22 eV above Γ_{15}. There is, however, no distinct maximum along ΓX close to the Γ point, as found in the earlier correlated Hartree–Fock calculation. The Cd 4d to O 2p separation is 9.11 eV at the Γ point and the Cd 4d bands show a small splitting of 0.10 eV between the threefold degenerate Γ'_{25} and twofold degenerate Γ_{12} states, with the latter uppermost. This represents the natural ordering for an essentially ionic crystal field splitting. As is usual in Hartree–Fock calculations, the gap between the occupied valence band and the empty conduction band is too big: the direct gap between Γ_{15} in the O 2p valence band and Γ_1 at the bottom of the conduction band is 11.66 eV at the Γ point. The indirect gaps are 10.41 eV and 10.44 eV. However, even though the absolute values for the energy gaps are much too large, the difference between energies of direct and indirect gaps is roughly correct.

Table 1. Bandgaps and bandwidths for CdO.

	HF[a]	DF[a]	Correlated HF[b]	Experimental
Γ_{15}–Γ_1 O 2p–Cd 5s direct gap	11.66	1.61	6.56	2.28[c]
L_3–Γ_1 O 2p–Cd 5s indirect gap	10.41	0.39	6.07	0.84[c]
Σ_4–Γ_1 O 2p–Cd 5s indirect gap	10.44	0.47		1.09[c]
Upward dispersion in O 2p band Γ_{15} to L_3	1.25	1.21	0.49	1.44[c]
Upward dispersion in O 2p valence band Γ_{15} to Σ_4	1.22	1.13	—	1.17[c]
Γ_{15}–Γ_{12} O 2p–Cd 4d separation at Γ	9.11	5.79	—	—
Γ_{15}–Γ'_{25} Cd 4d splitting at Γ	0.10	0.22	—	—
O 2p bandwidth	4.71	4.05	8.20	5.5[a]
Mean binding energy of Cd 4d relative to VBM	10.3	7.1	12.1	9.4[a]

[a] Present work.
[b] [11].
[c] [1].

The density functional calculation gives band dispersions qualitatively similar to the Hartree–Fock calculation (figure 2). However, the Cd 4d to O 2p separation specified above has the much smaller value of 5.79 eV. At the same time there is more pronounced Cd 4d–O 2p mixing away from Γ. The upward dispersion in the topmost O 2p valence band reaches 1.21 eV at the L point and 1.13 eV midway along ΓK. The overall width of the O 2p bands is much smaller in the density functional calculation. The direct gap at the Γ point has a value of 1.61 eV. Indirect gaps of 0.39 eV and 0.47 eV are also found. These values are now very slightly less than experimental values. The difference between direct and indirect transition energies (corresponding to the upward dispersion of the valence bands) is remarkably well reproduced by the calculation.

The features of the two calculations are further illustrated by the partial density of states profiles shown alongside the dispersion curves in figure 1 and 2. The Cd 4d band has a

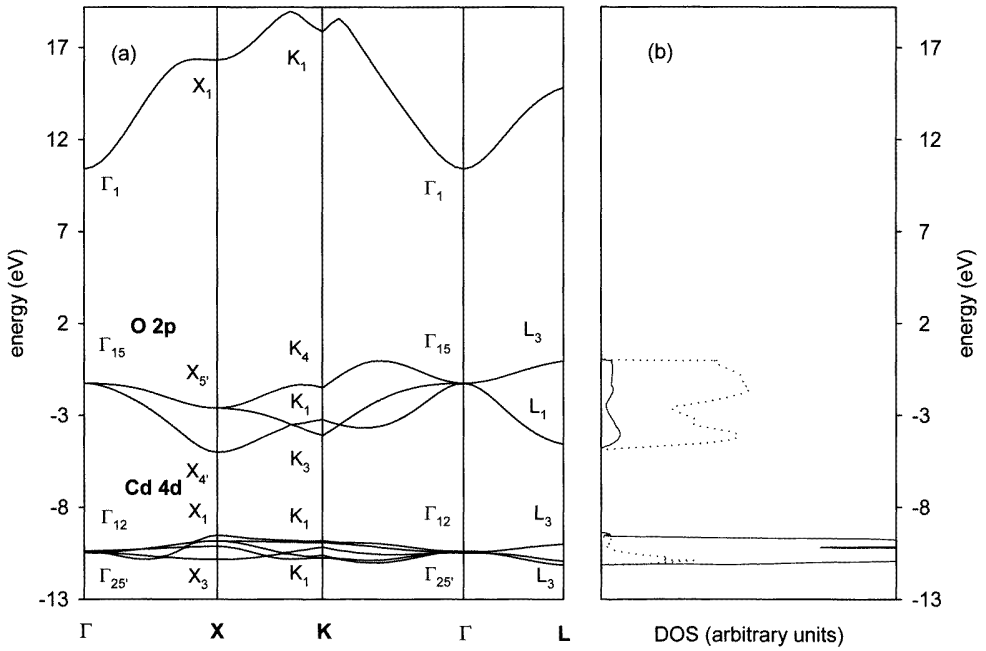

Figure 1. The band structure for CdO calculated by the periodic Hartree–Fock method. Symmetry labels for some of the bands at high-symmetry points are given. Alongside the band dispersions, the dashed curve shows the O 2p partial density of states and the full curve shows the Cd 4d partial density of states.

double peaked structure, with the centre of the spectral weight about 7.3 eV below the top of the O 2p valence band in the density functional calculation and 10.5 eV below in the Hartree–Fock calculation. The overall O 2p bandwidth is 4.05 eV in the density functional calculation and 4.71 eV in the Hartree–Fock calculation. The ratio between the Cd 4d contribution and the O 2p contribution to the density of states at the strongest maximum in the O 2p valence band is 0.15/0.85 in density functional theory, but only 0.08/0.92 in the Hartree–Fock calculation.

4.2. Comparison between XPS data and theoretical density of states profiles

Figure 3 shows the x-ray photoelectron spectrum of CdO in the region of the O 2p valence band and the Cd 4d level, along with theoretical densities of states. The binding energy scales in the calculations are referenced to the valence band maximum, whilst the binding energy scale for the experimental data is aligned so that the sharp peak at about 4 eV binding energy coincides with the corresponding peak in the Hartree–Fock calculation. An alternative reference for the experimental spectrum is provided by a weak but distinct Fermi–Dirac cut-off to low binding energy of the valence band. This arises from occupation of Cd 5s conduction band states associated with oxygen deficiency or cadmium interstitials. The Fermi level binding energy reference is essentially the same as that used by Vesely and Langer [12], who found that the Cd 4d peak maximum was at 12.20 eV binding energy relative to E_F. The position of the Fermi level relative to the valence band edge was not specified. In the present experiments we find the Cd 4d peak at a much lower binding

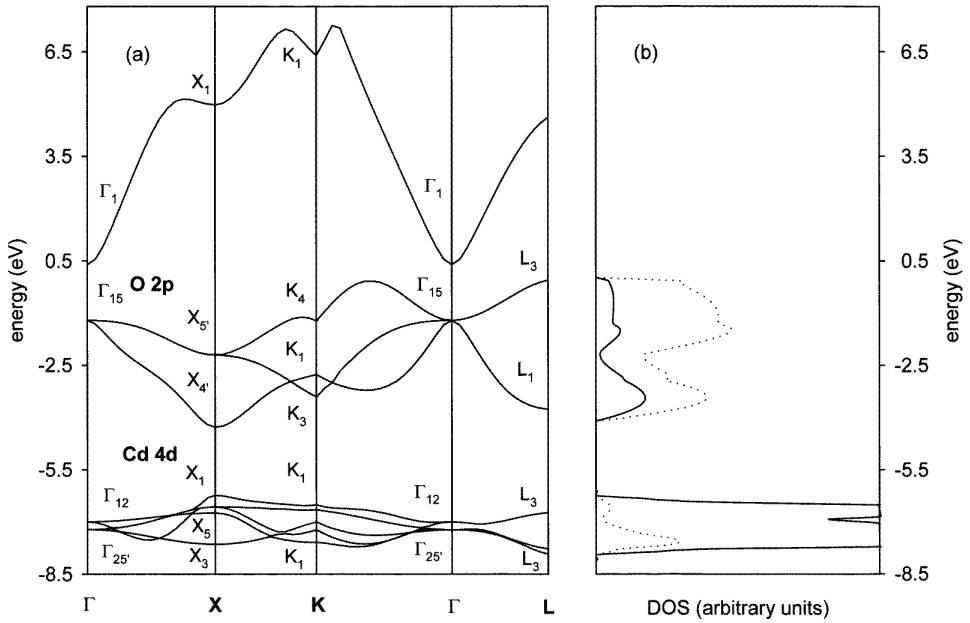

Figure 2. The band structure for CdO calculated by density functional theory. Symmetry labels for some of the bands at high-symmetry points are given. Alongside the band dispersions, the dashed curve shows the O 2p partial density of states and the full curve shows the Cd 4d partial density of states. Note that the overall energy spread is smaller than in figure 1.

energy of 10.7 eV relative to E_F. This earlier work used an uncleaned CdO sample in a spectrometer operating in the 10^{-6} mbar pressure range at 1.8 eV experimental resolution. It is probable that this sample was strongly contaminated with surface $CdCO_3$ or $Cd(OH)_2$. For these reasons we believe that the present data should be regarded as more reliable. Note, however, that there will be variation in binding energies depending on the carrier concentration of the CdO sample and hence the degree of filling of the O 2p conduction band [24]. In our case the carrier concentration after cleaning in UHV was estimated to be about 10^{20} cm^{-3}.

To facilitate comparison between the computed density of states profiles and the new XPS data it is necessary to take account of differences in ionization cross sections between O 2p and Cd 4d states. The one electron Cd 4d cross section at 1486.6 eV photon energy is estimated to be 2.6×10^{-3} Mb, whereas the corresponding O 2p cross section is only 6×10^{-5} Mb. It is therefore crucial to weight the partial densities of states with the photoionization cross sections [18]. This weighting is incorporated in figure 3. The figure shows that the Hartree–Fock calculation somewhat overestimates the O 2p—Cd 4d separation. However, the placement of the 4d level is much closer to the experimental value than in the earlier correlated Hartree–Fock calculation, which reported good agreement instead with the erroneous experimental data of Veseley and Langer [12]. In contrast to the Hartree–Fock calculation, the density functional calculation drastically underestimates the Cd 4d binding energy and the O 2p–Cd 4d separation. Focusing on the O 2p band shape, it is seen that the cross section weighted profile from the Hartree–Fock calculation is in good agreement with the experimental spectrum both in terms of the overall O 2p bandshape and bandwidth; and in the relative intensities of the two peaks in the spectral profile labelled *x*

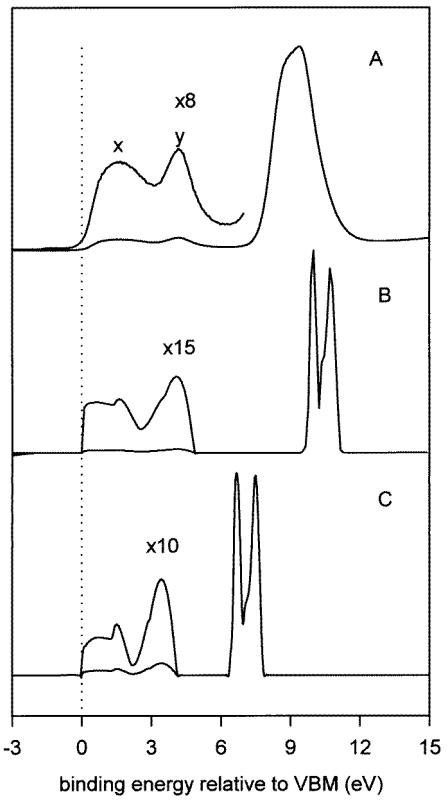

Figure 3. (A) An experimental x-ray photoemission spectrum of CdO in the region of the O 2p valence band and the Cd 4d shallow core level. (B) The cross section weighted density of states profile from the Hartree–Fock calculation. (C) The cross section weighted density of states profile from density functional theory. Binding energy scales in the calculated profiles are referenced to the upper edge of the O 2p valence band (see text for details). It is seen that the separation between the Cd 4d levels and the O 2p valence band is much better reproduced by the Hartree–Fock calculation than the density functional calculation.

and *y* in figure 3. The major discrepancy between the experimental and calculated profiles is that the valence band onset is much less sharp than that found in the calculation. This must be due in part to the finite experimental resolution as well as broadening of electronic structural features due to coupling with lattice phonons during the photoemission process. Figure 3 also shows a cross section weighted density of states profile from the density functional calculation. This method seriously underestimates the overall O 2p bandwidth and overestimates the intensity of peak *y* relative to peak *x*. This discrepancy can be traced to excessive mixing with Cd 4d states in the lower part of the valence band.

On balance then it appears that the Hartree–Fock calculation better reproduces the general features of the XPS of CdO. However, the direct and indirect bandgaps derived from density functional theory are in much better agreement with experimental values.

4.3. Vacuum UV photoemission

Photoemission spectra of polycrystalline CdO excited at the different vacuum UV photon energies indicated are shown in figure 4. Again well defined O 2p and Cd 4d bands are

observed, but at these lower energies the O 2p structure is much stronger relative to the Cd 4d structure than at higher photon energy. Bandwidths and band energies are in broad agreement with the XPS measurements, although the O 2p band shows a more complex spectral profile than under x-ray excitation. This could be due to a variety of factors including the existence of surface states. In the present discussion we concentrate on the CIS spectra shown in figure 5. These are taken over an energy window of 0.2 eV centred at the different binding energies indicated in figure 4.

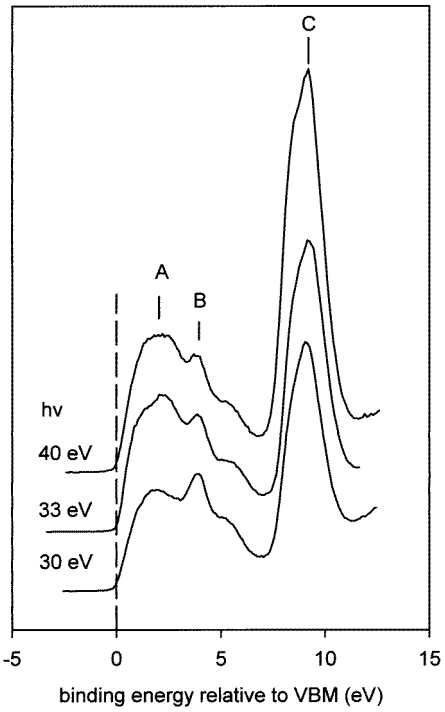

Figure 4. Photoemission spectra of polycrystalline CdO excited at the different photon energies indicated.

The CIS profile for states essentially in the middle of the Cd 4d band shows a very strong maximum at 50 eV photon energy. This is reproduced by the theoretical cross section calculated by Yeh and Lindau [18] using a central field approximation. The maximum is due to the strong centrifugal barrier experienced by the εf final states that provide the dominant continuum channel for ionization of the 4d electrons. The maximum in the Yeh–Lindau profile is shifted to a 10 eV lower photon energy compared with our experiment and the experimental profile is somewhat sharper than in the calculation. In addition, the experimental profile has a shoulder at around 65 eV photon energy. The shoulder corresponds roughly with the binding energy of the Cd 4p levels, as demonstrated by the shallow core x-ray excited photoemission spectrum of figure 6. (Note that the 4p spectrum is strongly influenced by many electron effects that lead to a complete breakdown of the one electron picture for the 4p core hole for Te [25]. The incipient many electron effects account for the broadness of the Cd 4p level.) This suggests that the shoulder is due to a resonance effect associated with 4p excitation. In transition metal compounds with partially occupied $n\mathrm{d}^m$ ($m < 10$) shells, resonance effects are associated with np to nd excitation,

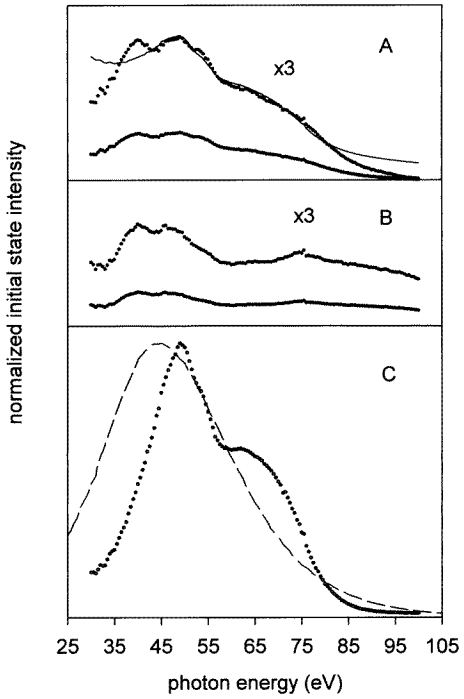

Figure 5. Constant initial-state spectra for polycrystalline CdO at two different points in the O 2p band and in the Cd 4d band, as indicated in figure 4. The dotted curves are experimental data. The dashed curve in C shows the Cd 4d cross section profile calculated by Yeh and Lindau. The full curve in A represents a cross section profile calculated by the Gelius model assuming 10% admixture of Cd 4d states into O 2p states.

followed by super-Coster–Krönig decay:

$$n\mathrm{p}^6 n\mathrm{d}^m + h\nu \rightarrow (n\mathrm{p}^5 n\mathrm{d}^{m+1})^*$$
$$(n\mathrm{p}^5 n\mathrm{d}^{m+1})^* \rightarrow n\mathrm{p}^6 n\mathrm{d}^{m-1} + \mathrm{e}.$$

This channel interferes with the direct ionization channel:

$$n\mathrm{p}^6 n\mathrm{d}^m + h\nu \rightarrow n\mathrm{p}^5 n\mathrm{d}^{m-1} + \mathrm{e}.$$

A characteristic Fano lineshape results.

In CdO the 4d shell is full so that this mechanism cannot operate in this simple way. Instead it is necessary to envisage excitation into conduction band states. These are of predominant Cd 5s atomic character, but there is admixture with both O 2p states and Cd 4d states. The wavefunction for conduction band state $|\mathrm{CB}\rangle$ may therefore be written in the form

$$|\mathrm{CB}\rangle = \alpha|\mathrm{Cd\ 5s}\rangle + \beta|\mathrm{O\ 2p}\rangle + \gamma|\mathrm{Cd\ 4d}\rangle$$

where $\alpha > \beta > \gamma$. In principle, there is also mixing with Cd 5p states, but this can be ignored for the present purposes. The presence of the γ weighted Cd 4d term and the large dipole matrix element between Cd 4p and Cd 4d states permits excitation of 4p electrons into conduction band states: there is an additional contribution to the excitation probability due to dipole excitation mediated by the matrix element between Cd 4p and Cd 5s states.

However, even though $\alpha \gg \gamma$, the former term is likely to predominate. The excited state with an electron in the conduction band can undergo Auger decay to a final state with a 4d shallow core hole:

$$4p^6 4d^{10} CB^0 + h\nu \rightarrow (4p^5 4d^{10} CB^1)^*$$
$$(4p^5 4d^{10} CB^1)^* \rightarrow 4p^6 4d^9 CB^0 + e.$$

Owing to the admixture of Cd 4d states into the conduction band, this decay has some super-Coster–Krönig character. The mechanism proposed here is similar to that used to account for resonantly enhanced Cu 3d satellites in the photoemission spectrum of the $3d^{10}$ oxide Cu_2O [26].

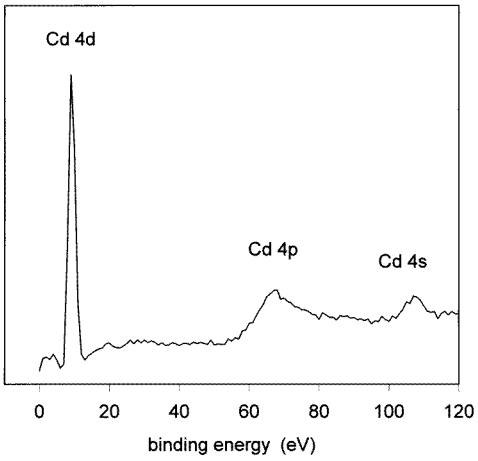

Figure 6. The Al K_α excited shallow core level photoemission spectrum of CdO showing the location of the Cd 4p levels.

The CIS profiles for O 2p valence band states both show maxima that are not expected from the pure O 2p cross section profile, which decreases monotonically across the range of photon energies investigated. This provides direct evidence for O 2p–Cd 4d mixing in the valence band states. We have attempted to interpret the data in terms of a Gelius-type model [27]. With this approach the ionization cross section for the hybridized O 2p–Cd 4d states may be written in the form

$$\sigma(\mathrm{VB}) = c_1\sigma(\mathrm{Cd\ 4d}) + c_2\sigma(\mathrm{O\text{–}2p})$$

where the coefficients c_1 and c_2 represent the relative magnitudes of the Cd 4d and O 2p partial density of states and the σ are one-electron ionization cross sections. The exact shape of the Cd 4d cross section profile is a crucial factor in the application of this model to our data. For this reason we first derive an empirical Cd 4d ionization cross section curve. This is done by normalizing the empirical CIS profile to have the same integrated intensity over the photon energy range between 30 eV and 100 eV. The curve is then corrected to allow for a small (10%) O 2p contribution to the Cd 4d states and rescaled to give a profile for states of 100% Cd 4d character. Finally, Cd 4d and O 2p states are mixed in differing proportions and cross section profiles are calculated for the hybridized states in accordance with the equation using the empirical curve for σ(Cd 4d) and the Yeh–Lindau curve for σ(O-2p). A major advantage of using the empirical Cd 4d profile is that we automatically correct for any errors in the normalization procedure used in deriving the CIS curves from

the raw experimental data. Figure 5 shows one example of the results of the analysis. With a Cd 4d contribution to the states at point C (figure 4) of the order 10%, a reasonable fit to the experimental data is achieved. The extent of Cd 4d mixing implied by this analysis is in reasonable agreement with the Hartree–Fock band structure calculation. A second weak peak in the valence band CIS curves at about 35 eV photon energy not reproduced by our analysis is possibly attributable to a resonance process involving O 2s excitation into conduction band states.

5. Concluding remarks

X-ray and UV photoemission spectra of polycrystalline CdO have been measured and are compared with Hartree–Fock and density functional calculations. The width of the O 2p band and the O 2p to Cd 4d separation are better reproduced by the Hartree–Fock calculation. The Hartree–Fock method deals in a natural way with the problem of self-interaction in the ground-state: the ability of a Hartree–Fock ground-state calculation to reproduce ionization energies is well known to arise from cancellation of errors in neglect of correlation and final-state relaxation. However, as is usual, the Hartree–Fock method does not deal adequately with the bandgap because correlation and relaxation errors augment each other in the treatment of affinity states, which therefore lie much too high in energy. Density functional theory, as implemented in the present paper, is not at all corrected for self-interaction. It deals less well than the Hartree–Fock model with the spread and detailed structure of the states produced by ionization of filled valence band levels. Of course, transition state models can be incorporated within density functional theory and this would lead to improved quantitative accuracy in the calculation of ionization energies.

The two theoretical calculations reported in the present paper both suggest that there is significant Cd 4d–O 2p mixing in CdO. This conclusion is confirmed by experimental constant initial-state spectra measured in the region of a maximum in the Cd 4d cross section profile. The separation between the inner nd states and the O 2p valence band states is bigger in CdO than in the neighbouring oxides ZnO and HgO, so the expectation is that hybridization of the nd levels with O 2p levels should be even more important in these oxides than in CdO.

Acknowledgments

We are grateful to assistance from S Downes in the UV photoemission measurements. YD is grateful to the Henry Lester Trust and the Great Britain-China Educational Trust for financial assistance

References

[1] Madelung O 1984 Landolt–Bornstein numerical data and functional relationships *Semiconductors: Physics of II-VI and I-VII Compounds, Semimagnetic Semiconductors Science and Technology* vol 17 (Berlin: Springer) part b
[2] Weiher R L and Ley R P 1966 *J. Appl. Phys.* **37** 299
[3] Jarzebski Z M and Marton J P 1976 *J. Electrochem. Soc.* **123** 299
[4] Srivastava V K and Chetal A R 1983 *Nuovo Cimento* **2D** 1014
[5] Abramov V N, Ermoshkin A N, Kuznezov A I and Murk V V 1984 *Phys. Status Solidi* B **12** K59
[6] Madelung O 1984 Landolt–Bornstein numerical data and functional relationships *Semiconductors: Physics of Non-Tetrahedrally Bonded Binary Compounds III Science and Technology* vol 17 (Berlin: Springer)
[7] Maschke K and Rossler U 1968 *Phys. Status Solidi* **28** 577

[8] Breeze A and Perkins P G 1973 *Solid State Commun.* **13** 1031
[9] Tewari S 1973 *Solid State Commun.* **12** 437
[10] Boettger J C and Kunz A B 1983 *Phys. Rev.* B **27** 1359
[11] Jaffe J E, Pandey R and Kunz A B 1991 *Phys. Rev.* B **43** 14 030
[12] Vesely C J and Langer D W 1971 *Phys. Rev.* B **4** 451
[13] Dunitz J D and Orgel L E 1960 *Adv. Inorg. Chem. Radiochem.* **2** 1
[14] Orchard A F and Richardson N V 1975 *J. Electron Spectrosc.* **6** 61
[15] Ivanov I and Pollmann J 1981 *Phys. Rev.* B **24** 7275
[16] Lee D H and Joannopoulos J D 1981 *Phys. Rev.* B **24** 6899
[17] Egdell R G, Orchard A F, Lloyd D R and Richardson N V 1977 *J. Electron Spectrosc.* **12** 415
[18] Yeh J J and Lindau I 1985 *At. Data Nucl. Data Tables* **32** 1
[19] Dovesi R, Saunders V R, Roetti C, Causà M, Harrison N M, Orlando R and Aprà E 1996 *CRYSTAL95 User's Manual* (Torino: Universà di Torino)
[20] von Barth U and Hedin L 1972 *J. Phys. C: Solid State Phys.* **5** 1629
[21] Perdew J P and Zunger A 1981 *Phys. Rev.* B **23** 5048
[22] Hehre W J, Radom L, Schleyer P R and Pople J A 1986 *Ab Initio Molecular Orbital Theory* (New York: Wiley)
[23] McCarthy M I and Harrison N M 1994 *Phys. Rev.* B **69** 8574
[24] Dou Y, Fishlock T, Egdell R G, Law D S L and Beamson G 1997 *Phys. Rev.* B **55** R13 381
[25] Wendin G and Ohno M 1976 *Physica Scr.* **14** 148
[26] Ghijsen J, Tjeng L H, Eskes H, Sawatzky G A and Johnson R L 1990 *Phys. Rev.* B **42** 2268
[27] Gelius U 1972 *Electron Spectroscopy* ed D Shirley (Amsterdam: North-Holland)